Adsorption of Rhodamine 6G Dye onto Al-MCM-41 and MCM-41 Mesoporous Materials

H. Douba, O. Mohammedi, and *B. Cheknane*[*]

Laboratory Physical Chemistry of Materials Interfaces Applied to the Environment,
University of Saad Dahlab Blida1, 09 000 Blida, Algeria

Abstract
The present study aimed to evaluate the potential of mesoporous silica MCM-41 and Al-MCM-41 (molar ratio Si/Al = 20) for the removal of Rhodamine 6G (Rh6G) from aqueous solution. The adsorbents were characterised by XRD, FTIR, SEM-EDX, BET, and UV-Raman. Obtained results related to XRD analysis indicated that the MCM-41 structure remained intact after the incorporation of Al species. Kinetic adsorption study showed that the higher removal (88.75 %, 26.62 mg g^{-1}) of Rh6G dye was achieved by Al-MCM-41 at 60 min. FTIR analysis showed that hydrogen bonding played the dominant role in the Rh6G removal mechanism, while the pH results showed that electrostatic interaction was also a key factor. This study shows that the prepared mesoporous materials are inexpensive and efficient adsorbents for the removal of cationic dyes.

Keywords
Adsorption, cationic dye, isotherms, mesoporous silica, Rhodamine 6G

1 Introduction

The greatest problem facing our world today is environmental pollution. Water and soil contain different kinds of pollutants, *i.e.*, heavy metal toxic ions,[1,2] antibiotics,[3] dyes, pesticides,[4] herbicides, *etc*. Rhodamine 6G (Rh6G) is a heterocyclic xanthene ring containing cationic dye having high solubility in aqueous medium,[5] it is the typical dye widely exploited as a colourant in cosmetics, textile, printing, and food manufacturing.[6,7] Rh6G dye is carcinogenic, neurotoxic, and causes chronic toxicity in humans and animals.[5] In addition, it may cause various health problems, such as irritation of eyes, skin, and respiratory tract.[6,8] In this sense, developing an effective method for the removal of Rh6G in wastewater is urgently needed.
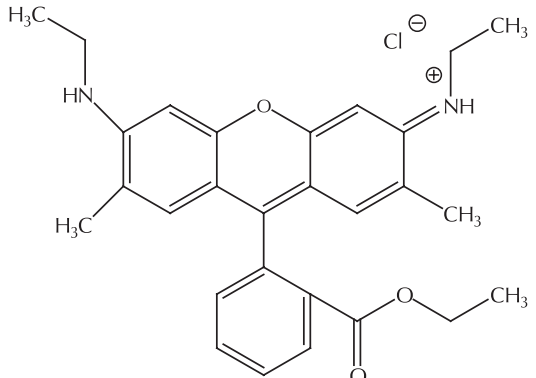
Reverse osmosis, ion exchange, precipitation,[6,9] electrocoagulation,[10] photodegradation,[11] photocatalyst,[12,13] electrochemical,[14] and adsorption[5,7] have been used for decolouration of Rh6G dye in aqueous systems. However, among these developed processes, it has been proved that the adsorption method is an effective purification technique due to its low cost, ease of operation, design, and environmentally friendly behaviour.[15,16] In addition, adsorption technology has shown its potential in removing different classes of dyes (ionic and molecular dyes) from industrial wastewater, and for single compound and multicomponent pollution.[17] Notably, among the adsorbents reported in previous research, the adsorption efficiency of Rh6G using these adsorbents is still limited because of their properties, nature and lower performance. In this regard, it is significant to develop a new effective and eco-friendly adsorbent to remove the toxic dye Rh6G from wastewater.

The new kind of nanostructured mesoporous materials of the M41S family, discovered by Mobil Corporation in 1992, has attracted intense interest due to well-ordered mesoporous materials with high surface area, controllable pore diameters (2–10 nm), and uniform structure of mesopores-channels.[18] In particular, MCM-41 as mesoporous material has been widely applied for cationic dyes adsorption in environmental wastewater, and is a promising adsorbent for the purification of organic contaminants.[19–23] Improving MCM-41 adsorption capacity and selectivity has attracted significant attention during the last decade.[24] In this context, the introduction of heteroatom or metal oxide into the MCM-41 structure was suggested, which is considered as one of the most effective approaches to enhance its sorption affinity to dye.[24–26] On the other hand, the integration of Al into the MCM-41 structure can lead to the formation of Brönsted acid sites. Thus, the adsorption affinity could be enhanced.[27] Similarly, *Dhal et al.*[24] evaluated the potential of iron oxide impregnation onto MCM-41 for methylene blue (MB) dye removal, and found a higher dye adsorption efficiency of 194 mg g^{-1} compared to the pure silica MCM-41, 149.5 mg g^{-1}. *Rashwan et al.*[28] prepared aluminosilicate cation exchanger Al-MCM-41 by wet-method to remove the MB from aqueous solution, and the results showed maximum monolayer adsorption ability. However, this method has some limitations, such as low surface area (592 m^2 g^{-1}) and ion exchange capacity, which has limited its applications. *Zanjanchi et al.*[29] studied the spectroscopic data of cationic dye loaded Al-MCM-41 (Si/Al = 5) materials at room temperature using aluminium sulphate source. However, the synthesis of this material at room temperature decreases the hydrothermal and structural stability.[30,31] In another research, Al-MCM-41 was synthesized by hydrothermal method, and showed a high affinity toward yellow dye molecules.[32] Compared to the aforementioned approaches, hydrothermal method is the easiest method to prepare MCM-41 and Al-MCM-41 with high stability and better ordered mesoporous structure. Consequently, the application of this material for the removal of other dyes could warrant research in the future.

[*] Corresponding author: Professor Benamar Cheknane
Email: ocheknane@yahoo.fr

Table 1 – Physical and chemical properties, and molecular structure of Rhodamine 6G (Rh6G) dye

Molecular name	Molecular formula	Molecular structure	Molecular weight / g mol^{-1}	Colour	Solubility in water / mg ml^{-1}
Rh6G (cationic dye)	$C_{28}H_{31}ClN_2O_3$		479.02	Red-brown	20

Thus, the main objective of this study was to examine the potential of mesoporous material as a low-cost adsorbent for the removal of cationic dye in aqueous solution. To the best of our knowledge, the performance of Al-MCM-41 and MCM-41 for Rh6G adsorption from aqueous solution with detailed mechanism has not been investigated previously.

In this study, mesoporous materials such as MCM-41 and Al-MCM-41 were prepared using hydrothermal method. The aluminium was integrated into the structure of MCM-41 by direct synthesis using aluminium isopropoxide with the molar ratio of Si/Al = 20. Due to the highly toxic Rh6G molecules that pollute water, the prepared mesoporous materials were used to remove this toxic dye from aqueous solution by batch adsorption experiments. The uptake capacity of the prepared adsorbents toward Rh6G under different factors, such as solution pH, contact time, Rh6G concentration, and temperature, was investigated. The non-linear modelling of kinetic and isotherm models were exploited to analyse adsorption kinetic data and test the equilibrium data, respectively. In addition, the thermodynamics of the adsorption was further investigated. Finally, the possible mechanism between Rh6G dye and the surface of mesoporous material was discussed.

2 Experimental

2.1 Materials

Tetraethyl orthosilicate (TEOS, 98 %, Sigma-Aldrich) was used as the silica source, hexadecyltrimethylammonium bromide (CTAB, ≥ 98 %, Sigma-Aldrich) was used as structure-directing agent, ammonium hydroxide solution (NH$_4$OH, 30 %, Sigma-Aldrich), and aluminium isopropoxide ([(CH$_3$)$_2$CHO]$_3$Al, ≥ 98 %, Sigma-Aldrich) was used as the aluminium source. Rh 6G was used as a probe for adsorption study. The physical and chemical properties and molecular structure of Rh6G are given in Table 1.

2.2 Synthesis of MCM-41

MCM-41 mesoporous silica was synthesized using a modified method from *Kumar et al.*[33] A quantity of 2.4 g of CTAB was dissolved in 120 ml of distilled water and stirred continuously to obtain a homogeneous solution. A volume of 8 ml of aqueous ammonia (30 wt. %) was added into the above solution. After 15 min under stirring, a known amount of silica source (TEOS) was added drop by drop into the mixture to prepare a gel with molar ratio of 1 TEOS: 0.15 CTAB: 1.64 NH$_4$OH: 126 H$_2$O. The designed homogeneous gel was transferred into an autoclave under hydrothermal treatment (100 °C for 72 h), after which the solution was collected by filtration and washed consecutively with distilled water. Finally, the sample was dried and calcined at 550 °C for 6 h in order to remove the trapped surfactant.

2.3 Synthesis of Al-MCM-41

Al-MCM-41 material was prepared according to the direct synthesis process in a molar ratio of Si/Al = 20. In a typical synthesis, a quantity of 2.4 g of CTAB was dissolved in 120 ml of distilled water at 25 °C and stirred continuously to obtain a clear homogeneous solution. A volume of 8 ml of aqueous ammonia (30 wt. %) was added into the solution. After 15 min, 10 ml of TEOS and aluminium isopropoxide (Si/Al = 20 molar ratio) were added into the mixture. The designed homogeneous gel was transferred into an autoclave under hydrothermal treatment (100 °C for 72 h). The solid was then filtered and the template was extracted by calcination at 550 °C for 6 h.

2.4 Characterisation

The two MCM-41 and Al-MCM-41 calcined materials were analysed using a PANalytical XPERT-PRO X-ray diffractometer with Cu Kα (λ = 0.154060 nm) radiation, operating at 45 kV and 30 mA. The vibrational properties of pure and aluminium-containing MCM-41 were investigated by both FTIR and UV-Raman spectroscopy. FTIR spectra were recorded using BRUKER ALPHA Platinum

ATR in the wavenumber range of 4000–400 cm^{-1}. UV–Raman spectroscopy measurements were carried out at room temperature using HORIBA Scientific LabRAM HR Evolution RAMAN SPECTROMETER system with a 325 nm excitation laser source and 2400 groove/mm grating. The surface morphology and chemical identity of both samples were characterised by scanning electron microscopy (FEI QUANTA 650) equipped with energy-dispersive X-ray spectroscopy (BRUKER X Flash 6/10). The specific surface area and porosity of the solids were studied by N$_2$ adsorption-desorption measurement at −196 °C (Quantachrome Instruments, Nova 1000e).

The pH at the point of zero charge (pH$_{PZC}$) is one of the most important factors in describing the ionisation behaviour of the adsorbent surface. In this study, 0.15 g of the adsorbent was added to 50 ml of 10^{-3} M NaCl solution. The initial pH value (pHi) of NaCl solution was adjusted to 2–11 by the addition of 0.1 M H$_2$SO$_4$ or 0.1 M NaOH. The mixture was agitated for 48 h at room temperature to reach equilibrium, and then the final pH (pHf) was measured. The pH$_{PZC}$ was obtained from the plot of pHi and pHf values.

2.5 Adsorption experiment

The standard batch process was used for adsorption experiments. The amount of 50 mg of adsorbent was added to 50 ml of Rh6G solution (30 mg l^{-1}) in a dark flask of 100 ml at pH 6.42, the resultant mixture was shaken with an orbital shaker (150 rpm) at room temperature for 5 h. The Rh6G solution was then centrifuged to separate Rh6G from the solid by FRONTIER™ 5706 centrifugation model. The supernatant was analysed by UV/Vis spectrophotometer at the maximum absorbance wavelength of 527 nm. The adsorption capacity (q_e, mg g^{-1}) and the removal efficiency (R, %) of Rh6G adsorbed on adsorbents at equilibrium were calculated using Eqs. (1) and (2), respectively.

$$q_e = \frac{(C_0 - C_e) \cdot V}{W} \tag{1}$$

$$R = \frac{(C_0 - C_e) \cdot 100 \text{ %}}{C_0} \tag{2}$$

where C_0 and C_e are the initial and equilibrium Rh6G concentrations (mg l^{-1}), respectively. V (l) is the initial volume of solution, and W (g) is mass of adsorbent.

The effect of variation of different adsorption parameters was investigated as a function of solution pH in the range 2–11, contact time (0–120 min), adsorbent dose (5–100 mg), and initial Rh6G concentration (2–80 mg l^{-1}). For thermodynamic studies, 25 mg of the adsorbent was added to 50 ml of Rh6G solution. The mixture was agitated in a thermostatic shaker bath at varying temperatures of 20, 30, 45, and 75 °C for 60 min.

2.6 Adsorption isotherm studies

Langmuir, Freundlich, Temkin, and Dubinin-Radushkevich models were used to describe the adsorption equilibrium

of Rh6G onto both adsorbents. The nonlinear equations of these isotherm models[34] are expressed by Eqs. (3)–(6).

$$\frac{K_L q_m C_e}{K_L C_e} \tag{3}$$

$$q_e = K_F C_e^{1/n} \tag{4}$$

$$q_e = \frac{RT}{b_t} \ln(K_T C_e) \tag{5}$$

$$q_e = q_{D-R} \exp(-\beta \varepsilon^2) \tag{6}$$

where C_e (mg l^{-1}) and q_e (mg g^{-1}) are the Rh6G concentration at equilibrium time and the adsorbent adsorption capacity, respectively. q_m (mg g^{-1}) is the maximum adsorption capacity, and K_L (l mg^{-1}) the Langmuir constant. $1/n$, K_F, and K_T are adsorption intensity coefficient, Freundlich constant, and Temkin constant, respectively. $RT/b_t = B$ is related to the heat of adsorption. q_{D-R} is the maximum adsorption capacity. E (kJ mol^{-1}) is the mean sorption energy, β is the activity coefficient, and ε is the Polanyi potential (kJ mol^{-1}), which are expressed by Eqs. (7) and (8), respectively.

$$\varepsilon = RT \ln\left(1 + \frac{1}{C_e}\right) \tag{7}$$

$$E = \frac{1}{\sqrt{2\beta}} \tag{8}$$

where R (8.314 J mol^{-1} K^{-1}) is the gas constant, and T (K) is the absolute temperature.

2.7 Kinetic studies

The pseudo-first-order, pseudo-second-order, intraparticle diffusion, and Elovich models were employed to evaluate the adsorption kinetics of Rh6G onto MCM-41 and Al-MCM-41. Nonlinear equations of these kinetic models[34] are expressed by Eqs. (9)–(12):

$$q_t = q_e \left(1 - \exp^{(-K_1 t)}\right) \tag{9}$$

$$q_t = \frac{K_2 q_e^2 t}{1 + K_2 q_e t} \tag{10}$$

$$q_t = K_{id} t^{1/2} + C \tag{11}$$

$$q_t = \frac{1}{\beta} \ln(1 + \alpha \beta \cdot t) \tag{12}$$

where q_e and q_t are the adsorption capacities (mg g^{-1}) at equilibrium and at time t, respectively. K_1 (min^{-1}) is the first-order kinetic rate constant, and K_2 (g mg^{-1} min^{-1}) is the pseudo-second-order kinetic rate constant. $K_2 q_e^2 = h$ is the initial adsorption rate (mg g^{-1} min^{-1}). K_{id} (mg g^{-1} min$^{-1/2}$) and C (mg g^{-1}) are the rate constant of intraparticle diffusion and the constant varied directly with the boundary layer thickness, respectively. α (mg g^{-1} min^{-1}) is the initial adsorption rate, and β (g mg^{-1}) is the extent of surface coverage.

3 Results and discussion

3.1 Characterisation

The small-angle XRD patterns of MCM-41 and Al-MCM-41 are given in Fig. 1. As shown in Fig. 1A, MCM-41 sample reveals a strong reflection peak (100) at $2\theta = 1.56°$ and three small peaks at $2\theta = 3.18°$, $3.74°$, and $5.27°$ correlate to (110), (200), and (210) reflections, respectively. The observed three well-resolved diffraction peaks (100), (110), and (200) confirmed the highly ordered and hexagonal mesoporous structure (space group *P6mm*) of MCM-41 type.[23,35] However, for Al-MCM-41, the reflection of (100) plane appeared at $2\theta = 2.30°$, and the presence of two small peaks at $2\theta = 3.59°$ (110) and $2\theta = 4.26°$ (200). The presence of three diffraction peaks confirmed the regular structure of the Al-containing MCM-41 sample with hexagonal symmetry. Indeed, as shown in Fig. 1B, the main reflection peak (100) became less intense and broader compared to MCM-41. As a result, the mesoporous structure of the MCM-41 sample was retained after the aluminium incorporation process.

Fig. 1 – Small angle X-ray diffraction patterns of: (A) MCM-41 and (B) Al-MCM-41

To study the surface morphology and composition of both mesoporous materials, scanning electron microscopy (SEM) images and energy dispersive X-ray (EDX) spectra prevailed, and the corresponding images SEM analysis are presented in Fig. 2 (A-B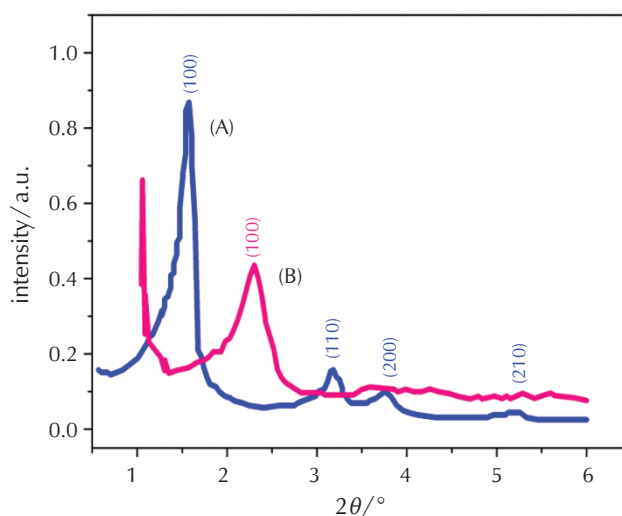). In both synthesized samples, the particles have a spherical morphology with particle size in the range of 0.4–0.7 μm. Furthermore, the morphology of the mesoporous material Al-MCM-41 was maintained during the synthesis process. The EDX spectroscopy study
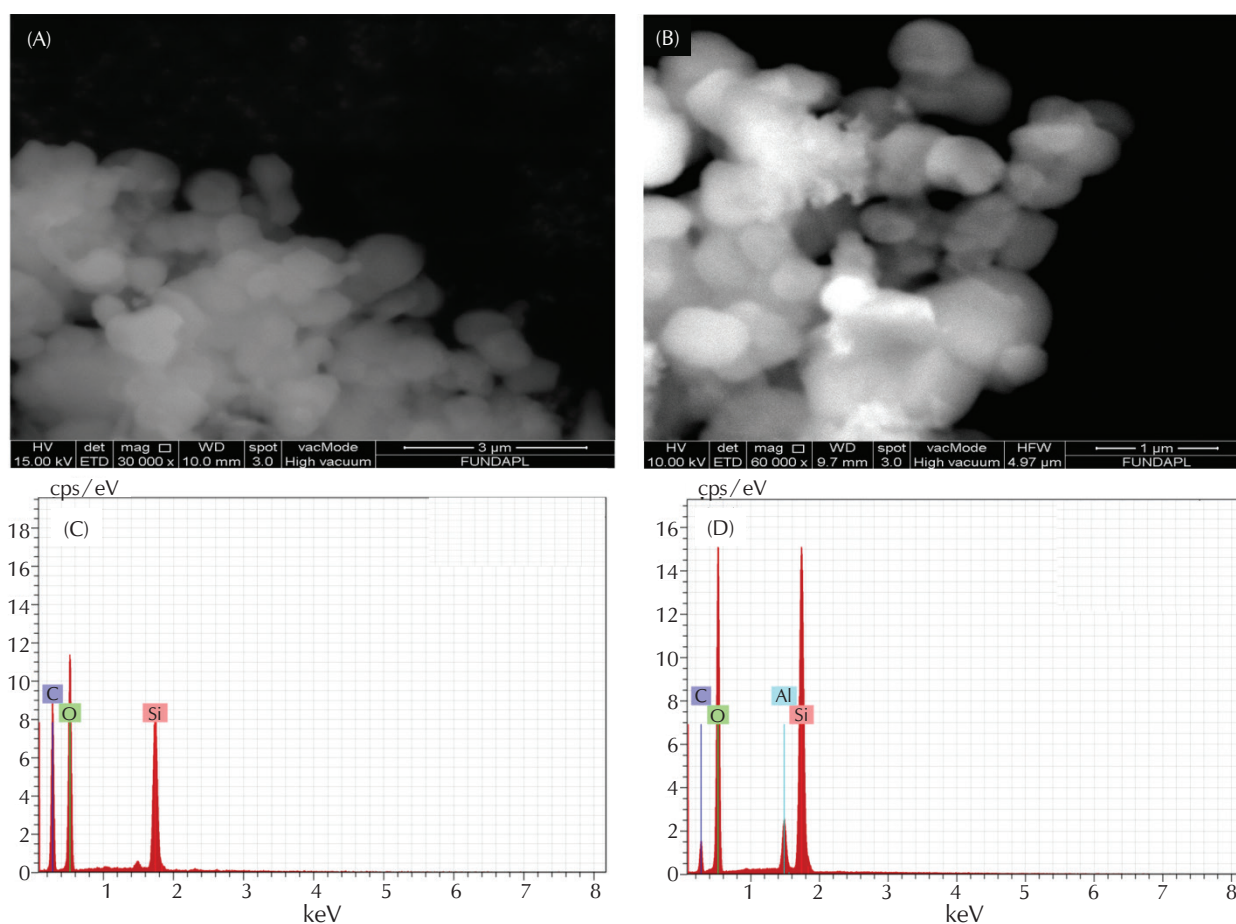

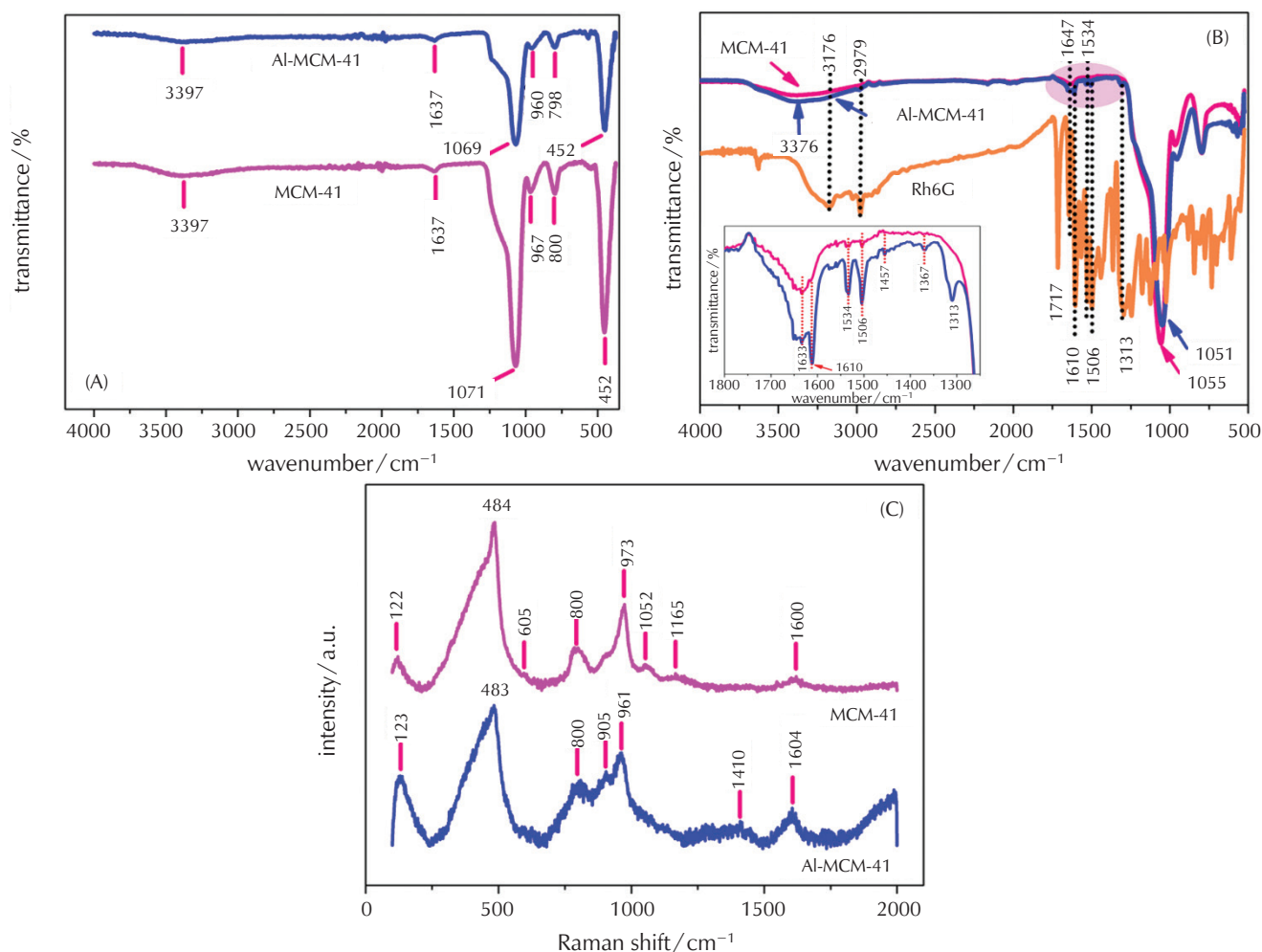*Fig. 2* – SEM images (A, B) and EDX spectra (C, D) of MCM-41 and Al-MCM-41, respectively

Fig. 3 – FTIR spectra (A) before, and (B) after Rh6G adsorption, and (C) UV Raman spectra of MCM-41 and Al-MCM-41

of Al-MCM-41, shown in Fig. 2D, suggested the presence of sharp peaks corresponding to Al, Si, C, and O atoms, indicating that the Al atom had incorporated into the surface of MCM-41 framework. Moreover, the peak of C in the spectrum was obtained from the carbon used during the preparation as a support of the sample. Therefore, the incorporation of aluminium into the mesoporous systems was confirmed by the EDX analysis (Fig. 2D).

FTIR spectra of MCM-41 and Al-MCM-41 before and after adsorption between 4000 and 450 cm^{-1} are shown in Fig. 3. The broad band about 3397 cm^{-1} may be assigned to stretching vibrations of water adsorbed on the surface and Si−OH silanol groups. In addition, a short peak at 1637 cm^{-1} is attributed to the H−O−H deformation vibration. The broad and most intense band at 1071 cm^{-1} is ascribed to the asymmetric stretching vibration of Si−O−Si, and a sharp band at 800 cm^{-1} corresponds to the symmetric stretching vibration of Si−O−Si. In addition, the intense band at 452 cm^{-1} is attributed to Si−O bending vibration. The typical bands of pure silica MCM-41 can be clearly observed on the spectra of Al-containing MCM-41, indicating the structure had been maintained. The absorption band at 960 cm^{-1} is usually attributed to the stretching vibrations of (Si−OH) or (Si−O−Al) vibration for hetero-

geneous metal loaded samples.[36] The displacement of the asymmetric stretching vibration band in the Al-MCM-41 is shifted toward lower wavenumbers (1069 cm^{-1}) compared with Si-MCM-41 (1071 cm^{-1}). This shift may have been caused by the incorporation of Al species into the framework of the mesostructure.

Based on Fig. 3B, the characteristic peak of pure Rh6G dye can be observed at 1313, 1610, and 2979 cm^{-1}, which is attributed to C−N stretching, C−C stretching in the aromatic ring, and C−H stretching, respectively.[37] The peak observed at 1647 cm^{-1} corresponds to the stretching vibration of carbonyl group (−COOH or −CONH) and N−H stretching vibration of amine groups.[38] Furthermore, the peaks at 1534 cm^{-1} and 1717 were assigned to C−N in-plane bending vibration and C=O stretching vibration of ester groups, respectively, and the band at about 3170 cm^{-1} was assigned to stretching vibration of the N−H secondary amine group, respectively.[39]

After Rh6G adsorption, the bands at 1069 and 1071 cm^{-1} shifted to lower wavenumber toward 1055 and 1051 cm^{-1} of MCM-41 and Al-MCM-41, respectively (Fig. 3B), indicating the interaction between Rh6G and adsorbent. Additionally, the band at 1637 cm^{-1} also shifted to lower
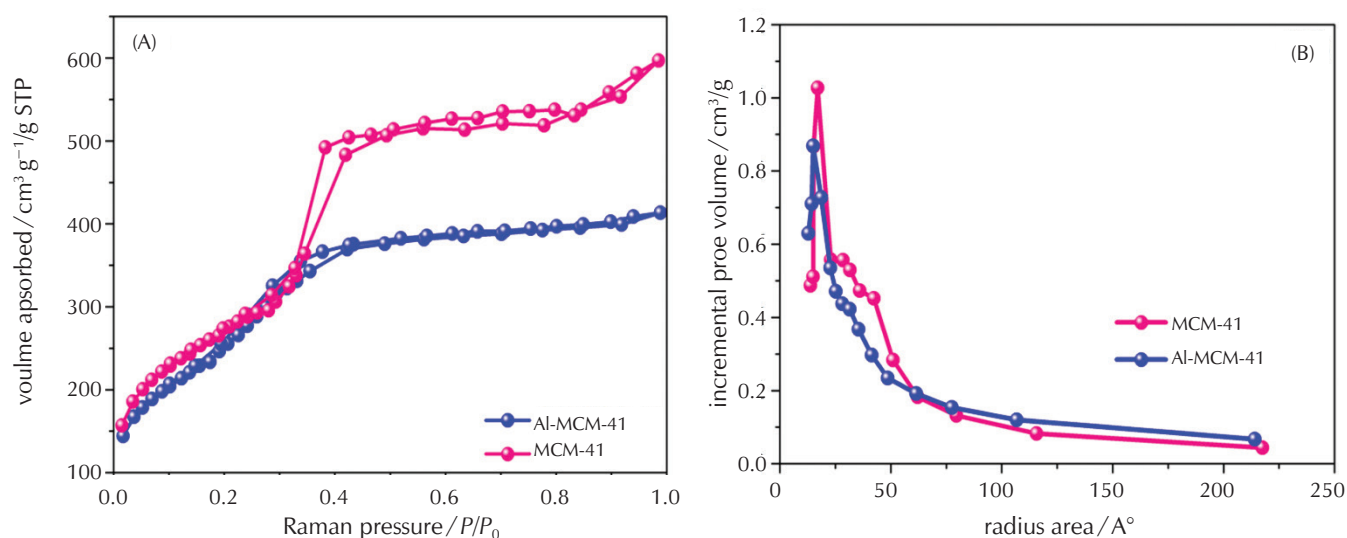
Fig. 4 – (A) Nitrogen adsorption-desorption isotherms, and (B) pore radius distribution obtained from the studied samples

wavenumber up to 1633 cm^{-1}, the −OH broad band at 3397 cm^{-1} also shifted to a lower wavenumber of approximately 3376 cm^{-1}. This phenomenon indicated that the hydrogen bonding between the amine groups of Rh6G with O−H groups of the mesoporous material surface was the dominant interaction mechanism. On the other hand, new bands were observed in the FTIR spectrum of Al-MCM-41 at 1610 cm^{-1} and at 2981 cm^{-1}, which corresponded to the C−C stretching of the aromatic ring and C−H stretching vibrations, respectively. This can probably be due to the existence of *n*-π interaction between Al-MCM-41 and Rh6G.[40] Hence, the shift and the presence of new bands confirmed that the Rh6G molecules had been successfully adsorbed onto the mesoporous material surface.

Raman spectroscopy is a complementary technique that can identify the vibration modes of these materials. The Raman spectra of Al-containing MCM-41 and pure silica MCM-41 in the range between 100 and 2000 cm^{-1} are given in Fig. 3C. In the spectrum of pure MCM-41, UV-Raman bands at 122, 484, 605, 800, 973, 1052, and 1600 cm^{-1} are clearly observed. The broad and most intense band around to 484 cm^{-1} is attributed to the asymmetric stretching vibrations of the Si−O−Si bond.[35,41] Otherwise, the less intense band at 800 cm^{-1} is associated with symmetric Si−O−Si stretching. However, Raman band at 973 cm^{-1} is associated with Si−OH stretching mode of vibrations of the surface silanol group.[42] Moreover, this band shifted to lower wavenumbers at 961 cm^{-1} after addition of Al species in the MCM-41 synthesis. This shift can be due to the interaction between Si−OH silanol groups and the aluminium oxide on the MCM-41 surface. UV–Raman analysis confirmed that the aluminium species had been successfully incorporated into the MCM-41 framework, which is in good agreement with the results observed by XRD, EDX and FT-IR analysis (Figs. 1–3).

In order to evaluate the textural properties, pore-size distribution, and surface area of both samples, N$_2$ adsorption-desorption analysis was performed. The N$_2$ adsorption-desorption isotherms and BJH pore-size distributions of two Al-MCM-41 and pure MCM-41 samples are given in Fig. 4. The BET surface areas, pore sizes, and pore volumes are also presented in Table 2.

The isotherms of both samples observed are typical for type IV adsorption/desorption pattern, corresponding to ordered mesoporous material.[43] BET surface area of pure silica MCM-41 was 998 m^2 g^{-1} with an average pore diameter of 3.4 nm. Compared to pure silica MCM-41, after aluminium incorporation, the BET surface area and average pore diameter decreased to 969 m^2 g^{-1} and 3.0 nm, respectively. Nevertheless, the pore volume of pure MCM-41 (0.38 cm^3 g^{-1}) was slightly higher than that of Al-MCM-41 (0.35 cm^3 g^{-1}).

Table 2 – Textural properties of MCM-41 and Al-MCM-41 samples

Sample	X-ray diffraction		N$_2$ adsorption			
	d_{100} spacing/ nm	Unit cell parameter, a_0[a] /nm	BET surface area/ m^2 g^{-1}	Pore volume/ cm^3 g^{-1}	Pore diameter, D_p /nm	Wall thickness[b] /nm
MCM-41	3.549	4.098	998	0.380	3.401	0.698
Al-MCM-41	3.321	3.835	969	0.350	3.021	0.835

[a] $a_0 = 2 \cdot d_{100}/\sqrt{3}$; d_{100} is the d-spacing of (100) reflection
[b] Wall thickness = $a_0 − D_p$.

3.2 Effect of pH

It is well known that the properties of the active sites of adsorbents and dye species during the adsorption reaction are affected by pH solution.[26] The effect of initial pH on equilibrium adsorption capacity of Rh6G using the mesoporous material was examined at varied pH from 2 to 11, and the results are given in Fig. 5A. At pH 2, the removal efficiency of Rh6G was very low, while the removal gradually increased with pH. Thus, lower adsorption of Rh6G at acidic pH is probably due to the presence of H$^+$ ions competing with the positively charged dye molecules for adsorption sites. The increase in Rh6G adsorption capacity with increasing pH (Fig. 5A), suggested the presence of more Si−O$^-$ due to the deprotonation of silanol groups, which caused a strong electrostatic interaction between the Rh6G dye ion and adsorbent.[44]

On the other hand, in alkaline solution at pH 11, the adsorption capacity of the cationic dye adsorbed was decreased. This fact can be explained by the interaction of dye with hydroxyl groups appearing to be the prevalent element. A study evaluated by *Mathew et al.*[45] showed that all dyes, including metanil yellow (MY), methylene blue (MB) and Rh6G, possess a maximum adsorption capacity on succinamic acid-functionalised MCM-41 (SA-MCM-41) observed at pH = 7, where the effect of pH was not important. As displayed in Fig. 5A, the maximum adsorption capacity for Rh6G was observed at pH 6.42 and 9 for Al-MCM-41 and pure silica MCM-41, respectively, but a slight difference was observed at pH 6.42 and 9 for MCM-41. From these results, other adsorption experiments were carried out with a neutral pH of the dye solution.

Another important factor for interpretation of the adsorption process of Rh6G is the point of zero charge (pH$_{PZC}$) of the adsorbent surface. The PZC is pH value at which the net total charge on MCM-41 surface is zero. When pH was lower than the pH$_{PZC}$ (pH < pH$_{PZC}$), the global surface charge on MCM-41 was positive, which reduced the removal efficiency of cationic dyes Rh6G. Conversely, at pH > pH$_{PZC}$, the surface was negatively charged, which was further favourable for the removal efficiency of cationic dyes. In this study, the pH$_{PZC}$ values of Al-MCM-41 and pure silica MCM-41 were estimated to be 4.48 and 6.38, respectively (Fig. 5B). Consequently, these results clearly indicated that, when the pH was greater than pH$_{PZC}$ (pH > 4.48), deprotonation of the Al-MCM-41 surface (Si−O$^-$) occurred, resulting in a strong electrostatic attraction between the positively charged Rh6G with the negative surface of Al-MCM-41.

3.3 Effect of adsorbent dose

To study the effect of adsorbent dose of mesoporous silica MCM-41 and Al-MCM-41 on Rh6G adsorption, 8 different dosages between 5 to 100 mg were investigated. According to Fig. 6B, the adsorption efficiency increased linearly with the increase in the amount of adsorbent until it reached maximum adsorption efficiency at 25 mg. In our study, the amount of 25 mg was selected as the optimum adsorbent dose.

3.4 Effect of contact time and adsorption kinetic

Contact time is one of the very important factors in the adsorption process. The influence of contact time on Rh6G adsorption of both MCM-41 and Al-MCM-41 adsorbents was studied for different times (0–120 min) at room temperature. The effects of contact time on Rh6G adsorption capacity are given in Fig. 6A. It is clear that the rate of adsorption was very quick, and afterward decreased gradually with time until adsorption reached equilibrium. This result was assigned to the progressive saturation of the adsorption sites of mesoporous material. According to Fig. 6A, Al-MCM-41 displayed excellent affinity for Rh6G dye removal in aqueous solution compared to MCM-41, which indicated a strong interaction between Rh6G and Al-MCM-41. In our study, the time of 60 min was selected
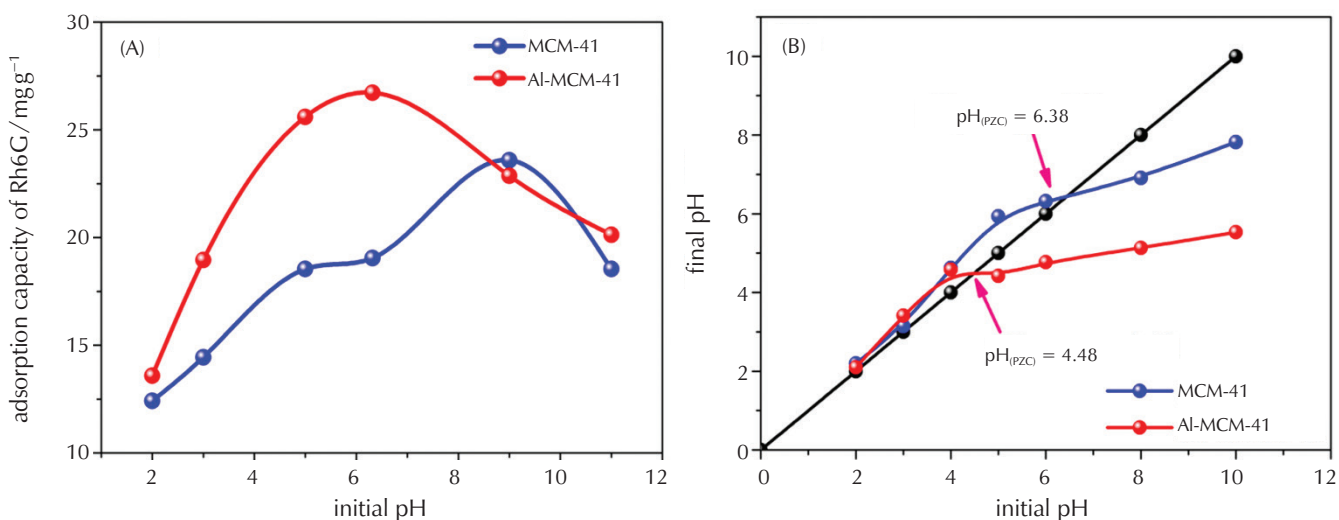

Fig. 5 – (A) Effect of pH on the adsorption capacity of Rh6G, and (B) point of zero charge (pHpzc) of MCM-41 and Al-MCM-41

as the optimum contact time to assure that equilibrium is achieved.

Adsorption kinetics is one of the more important features in defining the efficiency of pollutants adsorption process. To understand most of the mechanism of the adsorption process of Rh6G onto both mesoporous materials, four kinetic models were studied: pseudo-first-order, pseudo-second-order, intraparticle diffusion, and the Elovich models. The calculated parameters of these models by nonlinear regression analysis method, as well as correlation coefficients (R^2), are presented in Table 3, and the plots in Fig. 7.

Based on the correlation coefficients (R^2) of the kinetic models, the R^2 value of the pseudo-second-order kinetic model was much higher compared to the other models (Table 3), which was 0.999 close to unit for both adsorbents. Besides, the value of calculated adsorption capacity ($q_{e,cal}$) and experimental adsorption capacity ($q_{e,exp}$) were very close compared to $q_{e,cal}$ for pseudo-first-order kinetic model. Therefore, the pseudo-second-order model was the best-fitted kinetic model with satisfactory correlation coefficients. Similar results were reported for the removal of Rh6G on different adsorbents.[46,47]

Table 3 – Kinetic modelling for the adsorption of Rh6G in aqueous solution

| Model	Parameter	MCM-41	Al-MCM-41
Pseudo-first-order	K_1/min^{-1}	1.63	1.81
	$q_{e,exp}/\text{mg g}^{-1}$	18.98	26.62
	$q_{e,cal}/\text{mg g}^{-1}$	18.23	25.78
	R^2	0.978	0.991
Pseudo-second-order	$K_2/\text{g mg}^{-1}\text{min}^{-1}$	0.18	0.16
	$q_{e,cal}/\text{mg g}^{-1}$	18.73	26.38
	R^2	0.995	0.999
	$h/\text{mg g}^{-1}\text{min}^{-1}$	62.39	114.56
Intraparticle diffusion	$K_{id1}/\text{mg g}^{-1}\text{min}^{-0.5}$	2.11	2.77
	$C_1/\text{mg g}^{-1}$	12.70	19.03
	R^2	0.983	0.963
	$K_{id2}/\text{mg g}^{-1}\text{min}^{-0.5}$	0.16	0.17
	$C_2/\text{mg g}^{-1}$	17.62	25.24
	R^2	0.795	0.837
Elovich	$\alpha \cdot 10^{-8}/\text{mg g}^{-1}\text{min}^{-1}$	0.02	7.84
	$\beta/\text{g mg}^{-1}$	1.11	0.90
	R^2	0.994	0.996
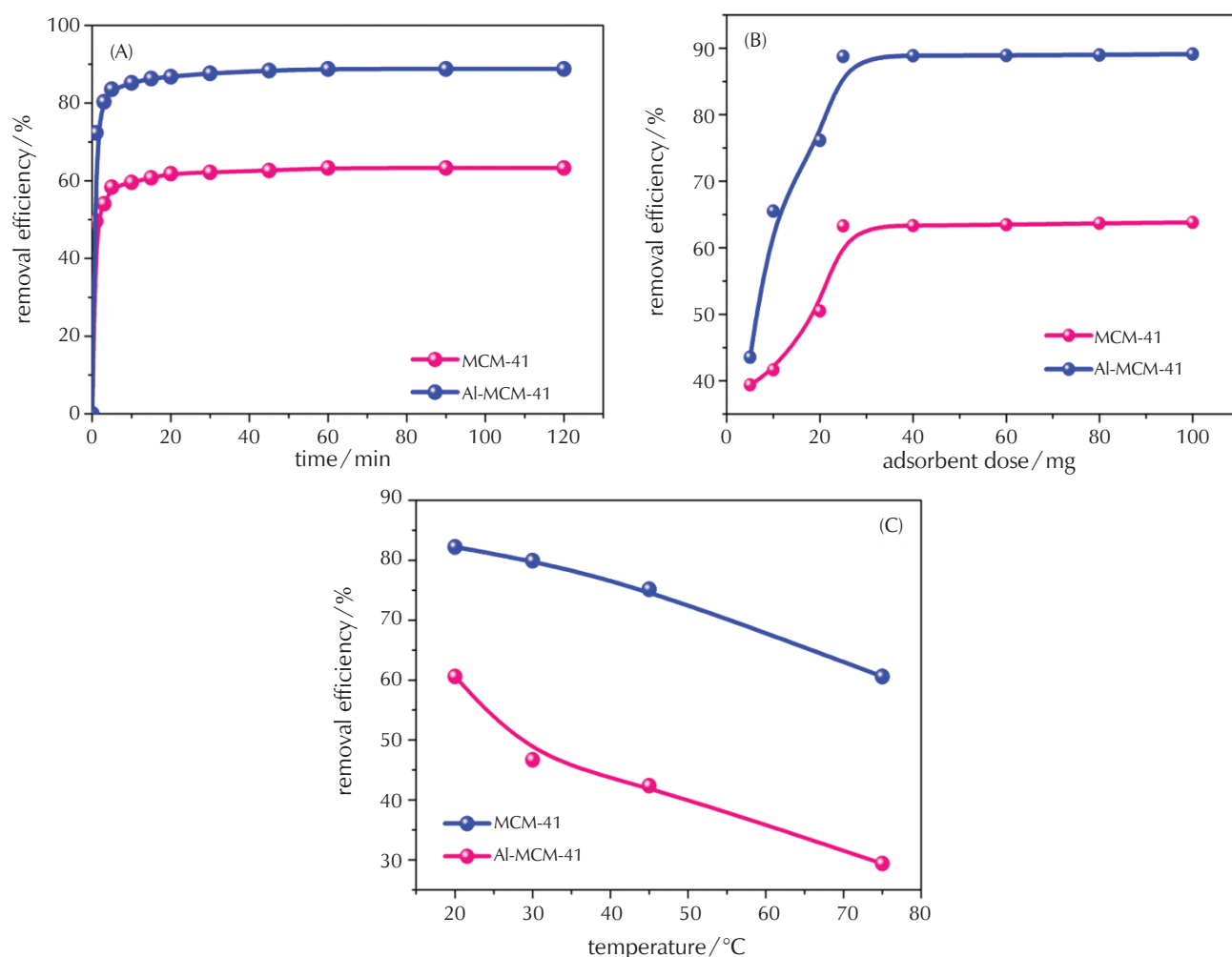
Fig. 6 – Variation in removal efficiency of Rh6G, (A) effect of contact time, (B) effect of adsorbent dose, and (C) effect of temperature
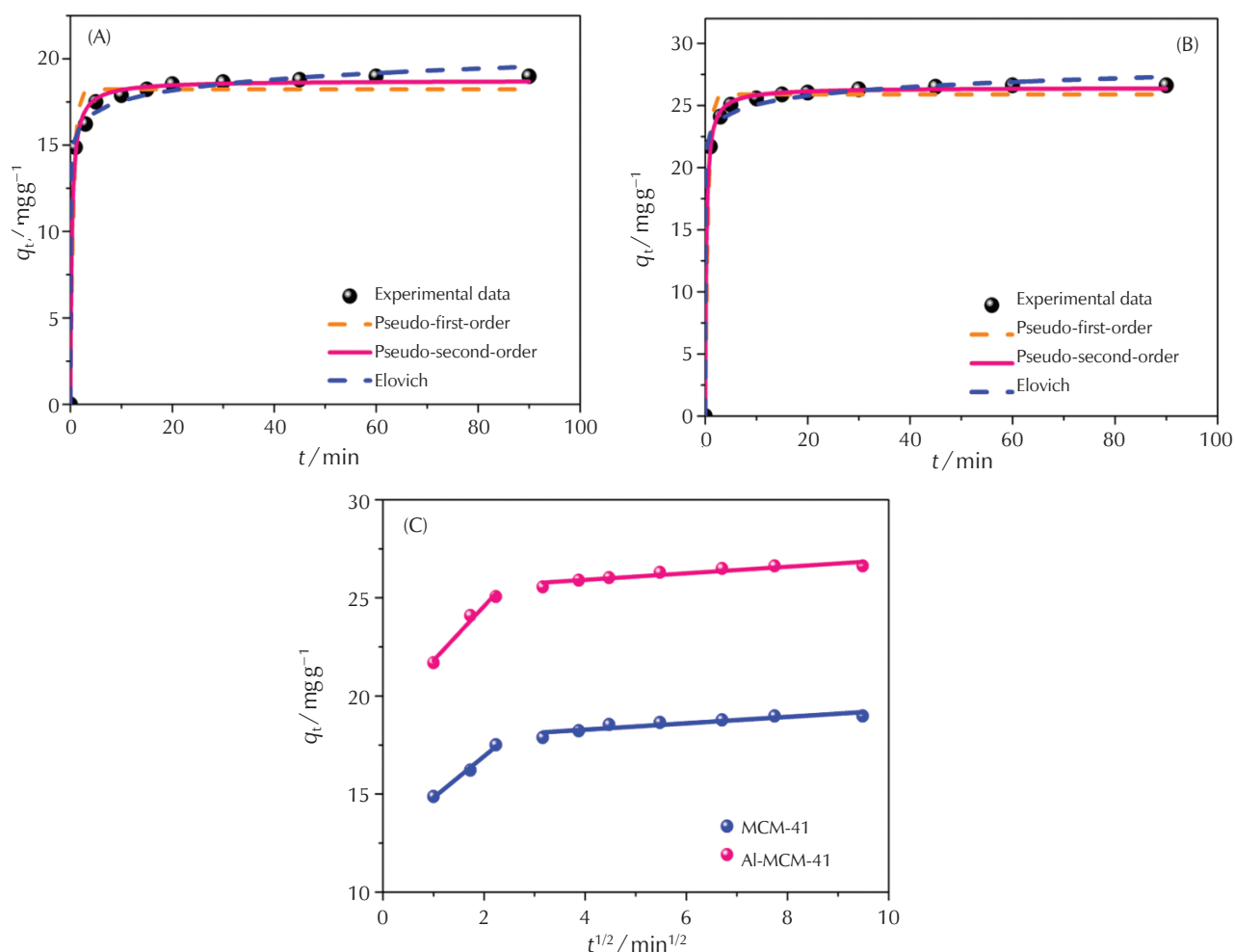
Fig. 7 – Experimental data and nonlinear fitting to three kinetic models for the adsorption of Rh6G by (A) MCM-41, (B) Al-MCM-41, and (C) fitted data to the intraparticle diffusion model for both adsorbents

Based on the intraparticle diffusion model, if the plot of q_t *versus* $t^{1/2}$ is linear and passes through the origin, the intraparticle diffusion is the only rate-limiting step. On the contrary, the film diffusion might be involved in the adsorption system.[48,49] From Fig. 7C, intraparticle diffusion plot did not pass through the origin ($C \neq 0$), indicating that the intraparticle diffusion was not the only step controlling the rate of Rh6G dye adsorption. According to this plot, two clear stages were observed. The first step is the rapid external mass transfer, while the second step is a gradual adsorption process.

3.5 Adsorption isotherm

In order to interpret the experimental data, four models of equilibrium data, Langmuir, Freundlich, Temkin, and Dubinin-Radushkevich isotherm models were applied. The calculated parameters of these models by non-linear regression analysis method are given in Table 4, and the non-linear plots are presented in Fig. 8. The maximum adsorption capacities of pure MCM-41 and Al-MCM-41 calculated from the Langmuir isotherm model were found to be 96.01 and 187.39 mg g⁻¹, respectively.

Table 4 – Equilibrium modelling for adsorption of Rh6G onto MCM-41 and Al-MCM-41

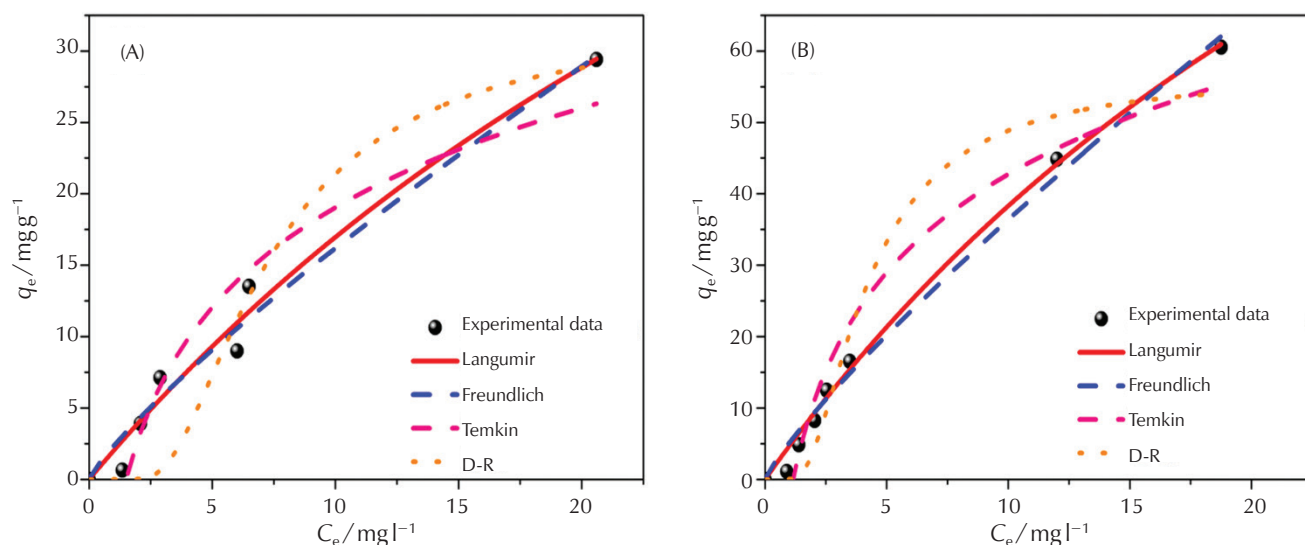| Isotherm	Parameters	MCM-41	Al-MCM-41
Langmuir	q_m/mg g⁻¹	96.01	187.39
	K_L/l mg⁻¹	0.02	0.03
	R^2	0.967	0.993
Freundlich	K_F/mg g⁻¹	2.36	5.14
	$1/n$	0.84	0.85
	R^2	0.963	0.988
Temkin	B	10.06	19.84
	K_T/l mg⁻¹	0.66	0.86
	R^2	0.924	0.960
Dubinin-Radushkevich	$\beta \cdot 10^6$/mol² J⁻²	7.25	2.59
	q_{D-R}/mg g⁻¹	32.04	56.45
	E/kJ mol⁻¹	0.26	0.44
	R^2	0.877	0.954

Fig. 8 – Experimental and nonlinear fitting to Langmuir, Freundlich, Temkin, and Dubinin-Radushkevich isotherms for Rh6G adsorption onto (A) MCM-41 and (B) Al-MCM-41

As displayed in Table 4, the correlation coefficient ($R^2 = 0.967$, 0.993) calculated from the Langmuir model was better than those calculated from D-R isotherm model ($R^2 = 0.848$, 0.946), Freundlich isotherm model ($R^2 = 0.962$, 0.988), and Temkin isotherm model ($R^2 = 0.906$, 0.953) onto MCM-41 and Al-MCM-41, respectively. These results clarify that the equilibrium isotherms data of Rh6G dye onto MCM-41 and Al-MCM-41, are better described by Langmuir isotherm models. Thus, it can be predicted that the adsorption of cationic dye Rh6G on the surface of MCM-41 type mesoporous materials follows the homogeneous monolayer adsorption.

In order to evaluate the feasibility of the adsorption process, the constant separation factor (R_L) was calculated from the following equation:[37]

$$R_L = \frac{1}{1 + K_L C_0} \tag{13}$$

The R_L values signify isotherm types: unfavourable ($R_L > 1$), irreversible ($R_L = 0$), favourable ($0 < R_L < 1$), and linear ($R_L = 1$). The calculated R_L values by this isotherm were found to be less than 1 and greater than 0, revealing the favourable adsorption nature of dye Rh6G onto both mesoporous materials. On the other hand, based on the concept of Freundlich, the values of n for the Rh6G uptake were found to be 1.17 and 1.19 for Al-MCM-41 and MCM-41, respectively. These values are at the limit of $1 < n < 10$, which indicates the better adsorption of the cationic dye Rh6G.[50]

The value of E is one of the most imperative parameters to evaluate the adsorption type. Furthermore, the physical or chemical type of adsorption process can be predicted depending on the energy value E, which was obtained from the Dubinin-Radushkevich isotherm model. The value of E should be lower than 8.0 kJ mol^{-1}, the adsorption process is physical in nature, but when the value of energy (E) is be-

tween 8 and 16.0 kJ mol^{-1}, the sorption process is chemical in nature.[51] The calculated energy E value was found to be 0.26 and 0.44 kJ mol^{-1} for pure MCM-41 and Al-MCM-41, respectively, which suggested that the adsorption process of cationic dye Rh6G was physical in nature. Similar results were found for the adsorption of cationic reactive dye.[23]
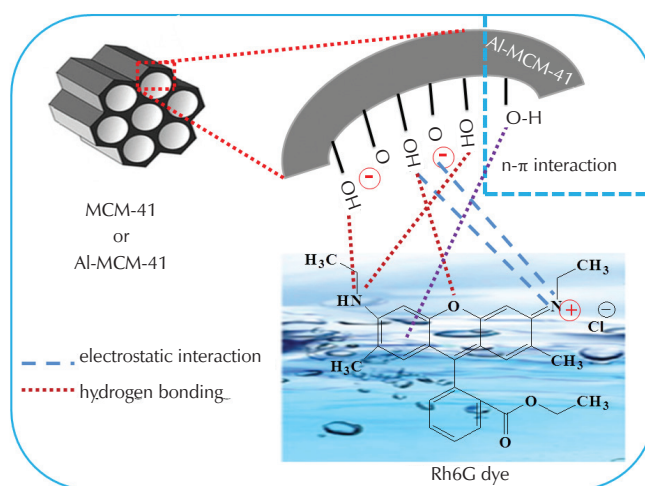

Fig. 9 – Proposed mechanism of Rhodamine 6G (Rh6G) dye onto mesoporous material

3.6 Adsorption mechanism

The possible interactions between Rh6G molecules and mesoporous material are presented in Fig. 9. The negative charge of MCM-41 and Al-MCM-41 surface due to the deprotonation of silanol (Si−O$^-$) groups can develop electrostatic interaction with the positive charge (−N$^+$) of Rh6G dye. According to the pH study, when the pH was greater than pH$_{PZC}$, the much higher adsorption of Rh6G

was mainly related to the electrostatic attraction of the cationic dye ($-N^+$) with the negative surface ($Si-O^-$) of Al-MCM-41.

According to the FTIR results, some significant changes on the adsorbent surface after Rh6G adsorption could be related to the interaction of Rh6G molecules with the mesoporous material surface through hydrogen bonding. Consequently, the amine groups ($-NHC_2H_5$) or oxygen atom ($-C-O-C-$) of Rh6G dye molecules could interact with the surface hydroxyl groups ($-OH$) of mesoporous material through hydrogen bonding, thus playing the dominant interaction mechanism. Hence, the mechanism of Rh6G dye from water onto both Al-MCM-41 and MCM-41 were found to result mainly from the electrostatic interaction and hydrogen bonding. Furthermore, the existence of n-π interaction between Al-MCM-41 and Rh6G dye can probably be involved. The oxygen groups of Al-MCM-41 could interact with the aromatic rings of Rh6G dye through n-π interaction.[40]

organisation and the decrease in randomness at the solid-solution interface during the adsorption process.[47,54]

Table 5 – Thermodynamic parameters associated with the adsorption process

Adsorbent	Temperature /°C	$\Delta G°$/kJ mol^{-1}	$\Delta H°$/ kJ mol^{-1}	$\Delta S°$/ J mol^{-1} K^{-1}
MCM-41	20	−0.71	−18.57	−60.97
	30	−0.10		
	45	0.81		
	75	2.64		
Al-MCM-41	20	−3.87	−17.19	−45.49
	30	−3.41		
	45	−2.73		
	75	−1.37		

3.7 Thermodynamic study

To study the effect of temperature, Rh6G adsorption studies were performed at different temperatures: 20, 30, 45, and 75 °C, during 60 min (Fig. 6C). The thermodynamic parameters, namely, the distribution coefficient (K_d), change of standard Gibbs free energy ($\Delta G°$), standard enthalpy change ($\Delta H°$), and standard entropy change ($\Delta S°$), were estimated by Eqs. (14)–(16).[15]

$$K_d = q_e/C_e \tag{14}$$

$$\Delta G° = -RT \ln K_d \tag{15}$$

$$\ln K_d = \Delta S°/R - \Delta H°/RT° \tag{16}$$

where T (K) is the absolute temperature, R is the gas constant, $\Delta S°$ and $\Delta H°$ values are calculated from Van't Hoff's equation (Eq. (16)) as the slope and intercept of ln K_d vs. $1/T$ plot. The calculated values of these parameters are given in Table 5.

$\Delta G°$ values (−1.37 to −3.87 kJ mol^{-1}) confirm the feasibility and spontaneous nature of Rh6G adsorption on the Al-MCM-41 adsorbent. Furthermore, the decrease of $\Delta G°$ negative value with increased temperature indicated that the adsorption of Rh6G was more favourable at lower temperature. In contrast, the positive value of $\Delta G°$ suggested the nonspontaneous nature of R6G adsorption onto pure silica MCM-41 adsorbent at 45 and 75 °C, which confirmed that the adsorption was spontaneous at lower temperature. The negative values of $\Delta H°$ shown in Table 5 suggest that the interaction of Rh6G adsorbed by the synthesized adsorbent was exothermic, confirming that the adsorption of Rh6G increased as the temperature decreased. Similar results have been reported for the removal of Rh6G by other adsorbents.[47,52] Consequently, the obtained absolute value of $\Delta H°$ was in the range of 17–20 kJ mol^{-1}, indicating the adsorption process to be physical in nature.[16,53] This result was in good agreement with those obtained by the value of E calculated from the R-D model (Table 4). Besides, the negative $\Delta S°$ value indicated the increase in the molecular

3.8 Comparison with other adsorbents

The maximum adsorption capacities for Rh6G uptake obtained from the Langmuir model by the materials of the current study and different adsorbents of the brief review are summarised in Table 6. It can be observed from this comparison that MCM-41 and Al-MCM-41 exhibited higher adsorption capacity for cationic Rh6G dye compared with other reported adsorbents. Obviously, Al-MCM-41 showed an excellent adsorption capacity (187.39 mg g^{-1}) for cationic dye Rh6G at room temperature. Therefore, it exhibits good removal ability for Rh6G.

Table 6 – Comparison of maximum adsorption capacity (q_{max}) of various adsorbents for Rh6G removal

Entry	Adsorbent	pH	q_{max}/ mg g^{-1}	Ref.
1	Pec-g-PHEAA	–	43.50	5
2	Pec-g-PHEAA/Fe$_3$O$_4$	–	57.20	5
3	Coffee ground powder	–	17.37	7
4	Activated carbon	7	44.70	55
5	Almond shell (*Prunus dulcis*)	8	32.60	46
6	Hexadecyl functionalised magnetic silica nanoparticles	9	35.60	47
7	Graphene oxide	–	23.30	39
8	Y type zeolite	5–6	9.90	37
9	PANI@TiO$_2$	Neutral	94	56
10	PANI@SiO$_2$	Neutral	61	56
11	Clitoria fairchildiana (CF)	6.4	73.84	53
12	Magnetic biochar (MB500)	7	9.42	54
13	MCM-41	6.4	96.01	This study
14	Al-MCM-41	6.4	187.39	This study

4 Conclusions

In this study, the prepared adsorbents were characterised by chemical and physical methods, and applied for removal of Rh6G from aqueous solution. BET surface area and average BJH pore diameter of pure silica MCM-41 decreased with the incorporation of aluminium species onto the surface of MCM-41. XRD analysis showed that the structure of Al-MCM-41 had been preserved during the incorporation process.

The kinetics of the adsorption process and isotherm data were best described by the pseudo-second-order kinetic (R^2 = 0.99) and Langmuir models. Al-MCM-41 showed a higher adsorption capacity of 187.39 mg g^{-1} than MCM-41 (96.01 mg g^{-1}) and other used adsorbents. Therefore, Al-MCM-41 material proved to be a potent and qualified adsorbent for the separation of Rh6G dye from wastewater. The study of intraparticle diffusion indicated that the adsorption phenomenon was not controlled by the intraparticle diffusion.

The spontaneous and exothermic nature of adsorption was demonstrated by the thermodynamic parameters. Moreover, the physical nature of Rh6G uptake was confirmed by the value of standard enthalpy change ($\Delta H°$) and the mean sorption energy E calculated from the Dubinin-Radushkevich model. The negative values of $\Delta S°$ (−45.49 to −60.97 J mol^{-1} k^{-1}) suggested that the randomness at the adsorbent/solution interface decreased during the adsorption of Rh6G. Based on the FTIR analysis, the Rh6G molecules were successfully adsorbed onto the surface of both mesoporous materials, confirming that hydrogen bonding was the dominant interaction mechanism, while the pH results showed that the electrostatic interaction was also a key factor. Consequently, the two mesoporous materials have enormous potential for the adsorption of cationic dyes.

References
Literatura

1. *F. Gokmen, E. Yaman, S. Temel*, Eco-friendly polyacrylic acid based porous hydrogel for heavy metal ions adsorption: characterization, adsorption behavior, thermodynamic and reusability studies, Microchem. J. **168** (2021) 106357, doi: https://doi.org/10.1016/j.microc.2021.106357.

2. *K. Nwosu-Obieogu, G. Dzarma, B. Okolo, K. Akatobi, F. Aguele,* Adsorption of Vanadium (V) From Textile Industry Effluent Using Luffa cylindrica Activated Carbon, Kem. Ind. **70** (3-4) (2021) 129–135, doi: https://doi.org/10.15255/KUI.2020.046.

3. *B. Wang, X. Xu, H. Tang, Y. H. Mao, Chen, F. Ji*, Highly ef-ficient adsorption of three antibiotics from aqueous solutions using glucose-based mesoporous carbon, Appl. Surf. Sci. **528** (2020) 147048, doi: https://doi.org/10.1016/j.apsusc.2020.147048.

4. *N. Gissawong, S. Mukdasai, S. Boonchiangma, S. Sansuk, S. Srijaranai*, A rapid and simple method for the removal of dyes and organophosphorus pesticides from water and soil samples using deep eutectic solvent embedded sponge, Chemosphere **260** (2020) 127590, doi: https://doi.org/10.1016/j.chemosphere.2020.127590.

5. *P. Kulal, V. Badalamoole*, Magnetite nanoparticle embedded Pectin-graft-poly (N-hydroxyethylacrylamide) hydrogel: Evaluation as adsorbent for dyes and heavy metal ions from wastewater, Int. J. Biol. Macromol. **156** (2020) 1408–1417, doi: https://doi.org/10.1016/j.ijbiomac.2019.11.181.

6. *T. Wang, P. Zhao, N. Lu, H. Chen, C. Zhang, X. Hou*, Facile fabrication of Fe$_3$O$_4$/MIL-101 (Cr) for effective removal of acid red 1 and orange G from aqueous solution, Chem. Eng. J. **295** (2016) 403–413, doi: https://doi.org/10.1016/j.cej.2016.03.016.

7. *K. Shen, M. Gondal*, Removal of hazardous Rhodamine dye from water by adsorption onto exhausted coffee ground, J. Saudi Chem. Soc. **21** (2017) S120–S127, doi: https://doi.org/10.1016/j.jscs.2013.11.005.

8. *J. Chen, X. Zhu*, Magnetic solid phase extraction using ionic liquid-coated core–shell magnetic nanoparticles followed by high-performance liquid chromatography for determination of Rhodamine B in food samples, Food Chem. **200** (2016) 10–15, doi: https://doi.org/10.1016/j.foodchem.2016.01.002.

9. *K. R. K. Reddy, Karthik, S. B. Prasad, S. K. Soni, H. M. Jeong, A. V. Raghu,* Enhanced photocatalytic activity of nanostructured titanium dioxide/polyaniline hybrid photocatalysts, Polyhedron **120** (2016) 169–174, doi: https://doi.org/10.1016/j.poly.2016.08.029.

10. *L. Zaleschi, M. S. Secula, C. Teodosiu, C. S. Stan, I. Cretescu,* Removal of rhodamine 6G from aqueous effluents by electrocoagulation in a batch reactor: assessment of operational parameters and process mechanism, Water Air Soil Pollut. **225** (9) (2014) 2101, doi: https://doi.org/10.1007/s11270-014-2101-z.

11. *M. d. L. R. Peralta, M. Sánchez-Cantú, E. Puente-López, E. Rubio-Rosas, F. Tzompantzi,* Evaluation of calcium oxide in Rhodamine 6G photodegradation, Catal. Today **305** (2018) 75–81, doi: https://doi.org/10.1016/j.cattod.2017.09.057.

12. *A. Chakraborty, D. A. Islam, H. Acharya,* Facile synthesis of CuO nanoparticles deposited zeolitic imidazolate frameworks (ZIF-8) for efficient photocatalytic dye degradation, J. Solid State Chem. **269** (2019) 566–574, doi: https://doi.org/10.1016/j.jssc.2018.10.036.

13. *W. d. S. Pereira, C. B. Gozzo, E. Longo, E. R. Leite, J. C. Sczancoski,* Investigation on the photocatalytic performance of Ag4P2O7 microcrystals for the degradation of organic pollutants, Appl. Surf. Sci. **493** (2019) 1195–1204, doi: https://doi.org/10.1016/j.apsusc.2019.07.148.

14. *N. Manjubaashini, P. J. Sephra, K. Nehru, M. Sivakumar, T. D. Thangadurai,* Electrochemical determination of ATP at rhodamine6G capped gold nanoparticles modified carbon felt electrode at pH 7.2, Sensor. Actuat. B–Chem. **281** (2019) 1054–1062, doi: https://doi.org/10.1016/j.snb.2018.10.149.

15. *R. Jayalakshmi, J. Jeyanthi,* Simultaneous removal of binary dye from textile effluent using cobalt ferrite-alginate nanocomposite: Performance and mechanism, Microchem. J. **145** (2019) 791–800, doi: https://doi.org/10.1016/j.microc.2018.11.047.

16. *H. Rezala, H. Douba, H. Boukhatem, A. Romero,* Adsorption of Methylene Blue by Hydroxyl-Aluminum Pillared Montmorillonite, J. Chem. Soc. Pakistan **42** (2020) 550–563, doi: https://doi.org/10.52568/000673/JCSP/42.04.2020.

17. *H. Mirzazadeh, M. Lashanizadegan,* Binary semiconductor oxide nanoparticles on graphene oxide ($CdO/CeO_2/RGO$) for the treatment of hazardous organic water pollutants, Korean J. Chem. Eng. **35** (3) (2018) 684–693, doi: https://doi.org/10.1007/s11814-017-0299-3.

18. *C. T. Kresge, M. E. Leonowicz, W. J. Roth, J. C. Vartuli, J. S. Beck,* Ordered mesoporous molecular sieves synthesized by a liquid-crystal template mechanism, Nature **359** (1992) 710–712, doi: https://doi.org/10.1038/359710a0.

19. *L.-C. Juang, C.-C. Wang, C.-K. Lee,* Adsorption of basic dyes onto MCM-41, Chemosphere **64** (11) (2006) 1920–1928, doi: https://doi.org/10.1016/j.chemosphere.2006.01.024.

20. *Q. Qin, J. Ma, K. Liu,* Adsorption of nitrobenzene from aqueous solution by MCM-41, J. Colloid Interf. Sci. **315** (1) (2007) 80–86, doi: https://doi.org/10.1016/j.jcis.2007.06.060.

21. *H. Chaudhuri, S. Dash, A. Sarkar,* Adsorption of different dyes from aqueous solution using Si-MCM-41 having very high surface area, J. Porous Mat. **23** (5) (2016) 1227–1237, doi: https://doi.org/10.1007/s10934-016-0181-4.

22. *M. Zhang, Y. Wu, Y. Fan, W. Zhu, H. Zhao, A. Arkin,* Evaluation of the mesoporous silica material MCM-41 for competitive adsorption of basic violet 5BN and basic green from industrial dye wastewater, Desalin. Water Treat. **57** (37) (2016) 17494–17511, doi: https://doi.org/10.1080/19443994.2015.1085448.

23. *A. J. Khan, J. Song, K. Ahmed, A. Rahim, P. L. O. Volpe, F. Rehman,* Mesoporous silica MCM-41, SBA-15 and derived bridged polysilsesquioxane SBA-PMDA for the selective removal of textile reactive dyes from wastewater, J. Mol. Liq. **298** (2020) 111957, doi: https://doi.org/10.1016/j.molliq.2019.111957.

24. *J. P. Dhal, T. Dash, G. Hota,* Iron oxide impregnated mesoporous MCM-41: synthesis, characterization and adsorption studies, J. Porous Mat. **27** (1) (2020) 205–216, doi: https://doi.org/10.1007/s10934-019-00803-0.

25. *Y. Shao, X. Wang, Y. Kang, Y. Shu, Q. Sun, L. Li,* Application of Mn/MCM-41 as an adsorbent to remove methyl blue from aqueous solution, J. Colloid Interf. Sci. **429** (2014) 25–33, doi: https://doi.org/10.1016/j.jcis.2014.05.004.

26. *Y. Shu, Y. Shao, X. Wei, X. Wang, Q. Sun, Q. Zhang, L. Li,* Synthesis and characterization of Ni-MCM-41 for methyl blue adsorption, Micro. Meso. Mater. **214** (2015) 88–94, doi: https://doi.org/10.1016/j.micromeso.2015.05.006.

27. *A. C. Carmo Jr, L. K. de Souza, C. E. da Costa, E. Longo, J. R. Zamian, G. N. da Rocha Filho,* Production of biodiesel by esterification of palmitic acid over mesoporous aluminosilicate Al-MCM-41, Fuel **88** (3) (2009) 461–468, doi: https://doi.org/10.1016/j.fuel.2008.10.007.

28. *W. E. Rashwan, K. S. Abou-El-Sherbini, M. A. Wahba, S. A. S. Ahmed, P. G. Weidler,* High stable Al-MCM-41: structural characterization and evaluation for removal of methylene blue from aqueous solution, Silicon (2019) 2017–2029, doi: https://doi.org/10.1007/s12633-019-00262-x.

29. *M. Zanjanchi, A. Ebrahimian, Z. Alimohammadi,* A spectroscopic study on the adsorption of cationic dyes into mesoporous AlMCM-41 materials, Opt. Mater. **29** (7) (2007) 794–800, doi: https://doi.org/10.1016/j.optmat.2005.12.008.

30. *H. I. Meléndez-Ortiz, A. Mercado-Silva, L. A. García-Cerda, G. Castruita, Y. A. Perera-Mercado,* Hydrothermal synthesis of mesoporous silica MCM-41 using commercial sodium silicate, J. Mex. Chem. Soc. **57** (2) (2013) 73–79, doi: https://doi.org/10.29356/jmcs.v57i2.215.

31. *Y. Ma, H. Chen, Y. Shi, S. Yuan,* Low cost synthesis of mesoporous molecular sieve MCM-41 from wheat straw ash using CTAB as surfactant, Mater. Res. Bull. **77** (2016) 258–264, doi: https://doi.org/10.1016/j.materresbull.2016.01.052.

32. *B. Boukoussa, R. Hamacha, A. Morsli, A. Bengueddach,* Adsorption of yellow dye on calcined or uncalcined Al-MCM-41 mesoporous materials, Arab. J. Chem. **10** (2017) S2160–S2169, doi: https://doi.org/10.1016/j.arabjc.2013.07.049.

33. *D. Kumar, K. Schumacher, C. d. F. von Hohenesche, M. Grün, K. Unger,* MCM-41, MCM-48 and related mesoporous adsorbents: their synthesis and characterisation, Colloid. Surface. A **187** (2001) 109–116, doi: https://doi.org/10.1016/S0927-7757(01)00638-0.

34. *A. C. Sadiq, N. Y. Rahim, F. B. M. Suah,* Adsorption and desorption of malachite green by using chitosan-deep eutectic solvents beads, Int. J. Biol. Macromol. **164** (2020) 3965–3973, doi: https://doi.org/10.1016/j.ijbiomac.2020.09.029.

35. *L. Kuboňová, P. Peikertova, K. M. Kutláková, K. Jirátová, G. Słowik, L. Obalova, P. Cool,* Catalytic activity of cobalt grafted on ordered mesoporous silica materials in N_2O decomposition and CO oxidation, Mol. Catal. **437** (2017) 57–72, doi: https://doi.org/10.1016/j.mcat.2017.04.037.

36. *H. Faghihian, M. Naghavi,* Synthesis of Amine-Functionalized MCM-41 and MCM-48 for removal of heavy metal ions from aqueous solutions, Sep. Sci. Technol. **49** (2) (2014) 214–220, doi: https://doi.org/10.1080/01496395.2013.819516.

37. *D. Viboonratanasri, S. Pabchanda, P. Prompinit,* Rapid and simple preparation of rhodamine 6G loaded HY zeolite for highly selective nitrite detection, Appl. Surf. Sci. **440** (2018) 1261–1268, doi: https://doi.org/10.1016/j.apsusc.2018.01.156.

38. *T. Atugoda, C. Gunawardane, M. Ahmad, M. Vithanage,* Mechanistic Interaction of Ciprofloxacin on Zeolite modified Seaweed (*Sargassum crassifolium*) derived Biochar: Kinetics, Isotherm and Thermodynamics, Chemosphere **281** (2021) 130676, doi: https://doi.org/10.1016/j.chemosphere.2021.130676.

39. *H. Ren, D. D. Kulkarni, R. Kodiyath, W. Xu, I. Choi, V. V. Tsukruk,* Competitive adsorption of dopamine and rhodamine 6G on the surface of graphene oxide, ACS Appl. Mater. Inter. **6** (4) (2014) 2459–2470, doi: https://doi.org/10.1021/am404881p.

40. *H. N. Tran, Y.-F. Wang, S.-J. You, H.-P. Chao,* Insights into the mechanism of cationic dye adsorption on activated charcoal: the importance of π–π interactions, Process Saf. Environ. **107** (2017) 168–180, doi: https://doi.org/10.1016/j.psep.2017.02.010.

41. *F. J. Méndez, O. E. Franco-López, X. Bokhimi, D. A. Solís-Casados, L. Escobar-Alarcón, T. E. Klimova,* Dibenzothiophene hydrodesulfurization with NiMo and CoMo catalysts supported on niobium-modified MCM-41, Appl. Catal. B–Environ. **219** (2017) 479–491, doi: https://doi.org/10.1016/j.apcatb.2017.07.079.

42. *W.-H. Zhang, J. Lu, B. Han, M. Li, J. Xiu, P. Ying, C. Li,* Direct synthesis and characterization of titanium-substituted mesoporous molecular sieve SBA-15, Chem. Mater. **14** (8) (2002) 3413–3421, doi: https://doi.org/10.1021/cm011686c.

43. *K. H. Kim, D. J. Lee, K. M. Cho, S. J. Kim, J.-K. Park, H.-T. Jung,* Complete magnesiothermic reduction reaction of vertically aligned mesoporous silica channels to form pure silicon nanoparticles, Sci. Rep. **5** (1) (2015) 9014, doi: https://doi.org/10.1038/srep09014.

44. *X. Han, Y. Wang, N. Zhang, J. Meng, Y. Li, J. Liang,* Facile synthesis of mesoporous silica derived from iron ore tailings for efficient adsorption of methylene blue, Colloid. Surface. A **617** (2021) 126391, doi: https://doi.org/10.1016/j.colsur-

fa.2021.126391.

45. *A. Mathew, S. Parambadath, M. J. Barnabas, H. J. Song, J.-S. Kim, S. S. Park, C. S. Ha,* Rhodamine 6G assisted adsorption of metanil yellow over succinamic acid functionalized MCM-41, Dyes Pigm. **131** (2016) 177–185, doi: https://doi.org/10.1016/j.dyepig.2016.04.007.

46. *H. B. Senturk, D. Ozdes, C. Duran,* Biosorption of Rhodamine 6G from aqueous solutions onto almond shell (*Prunus dulcis*) as a low cost biosorbent, Desalination **252** (2010) 81–87, doi: https://doi.org/10.1016/j.desal.2009.10.021.

47. *Y. P. Chang, C. L. Ren, Q. Yang, Z. Y. Zhang, L. J. Dong, X. G. Chen, D. S. Xue,* Preparation and characterization of hexadecyl functionalized magnetic silica nanoparticles and its application in Rhodamine 6G removal, Appl. Surf. Sci. **257** (2011) 8610–8616, doi: https://doi.org/10.1016/j.apsusc.2011.05.031.

48. *S. Zhang, Y. Dong, Z. Yang, W. Yang, J. Wu, C. Dong,* Adsorption of pharmaceuticals on chitosan-based magnetic composite particles with core-brush topology, Chem. Eng. J. **304** (2016) 325–334, doi: https://doi.org/10.1016/j.cej.2016.06.087.

49. *J. Jin, T. Feng, Y. Ma, W. Wang, Y. Wang, Q. Zhou, A. Li,* Novel magnetic carboxyl modified hypercrosslinked resins for effective removal of typical PPCPs, Chemosphere **185** (2017) 563–573, doi: https://doi.org/10.1016/j.chemosphere.2017.07.058.

50. *H.-M. Yang, S.-C. Jang, S. B. Hong, K.-W. Lee, C. Roh, Y. S. Huh, B. K. Seo,* Prussian blue-functionalized magnetic nanoclusters for the removal of radioactive cesium from water, J. Alloy. Compd. **657** (2016) 387–393, doi: https://doi.org/10.1016/j.jallcom.2015.10.068.

51. *A. Q. Selim, E. A. Mohamed, M. Mobarak, A. M. Zayed, M. K. Seliem, S. Komarneni,* Cr (VI) uptake by a composite of processed diatomite with MCM-41: Isotherm, kinetic and thermodynamic studies, Micropor. Mesopor. Mat. **260** (2018) 84–92, doi: https://doi.org/10.1016/j.micromeso.2017.10.041.

52. *N. Jarrah,* Competitive adsorption isotherms of rhodium 6G and methylene blue on activated carbon prepared from residual fuel oil, J. Environ. Chem. Eng. **5** (5) (2017) 4319–4326, doi: https://doi.org/10.1016/j.jece.2017.08.006.

53. *A. M. B. da Silva, N. O. Serrão, G. de Gusmão Celestino, M. L. Takeno, N. T. B. Antunes, S. Iglauer, L. Monzato, F. A. de Freitas, P. J. D. Maia,* Removal of rhodamine 6G from synthetic effluents using Clitoria fairchildiana pods as low-cost biosorbent, Environ. Sci. Pollut. R. **27** (3) (2020) 2868–2880, doi: https://doi.org/10.1007/s11356-019-07114-6.

54. *T. Suwunwong, P. Patho, P. Choto, K. Phoungthong,* Enhancement the rhodamine 6G adsorption property on Fe_3O_4-composited biochar derived from rice husk, Mater. Res. Express **7** (2020) 025511, doi: https://doi.org/10.1088/2053-1591/ab6b58.

55. *G. Annadurai, R.-S. Juang, D.-J. Lee,* Adsorption of rhodamine 6G from aqueous solutions on activated carbon, J. Environ. Sci. Heal. A **36** (5) (2001) 715–725, doi: https://doi.org/10.1081/ESE-100103755.

56. *M. Maruthapandi, L. Eswaran, J. H. Luong, A. Gedanken,* Sonochemical preparation of polyaniline@TiO_2 and polyaniline@SiO_2 for the removal of anionic and cationic dyes, Ultrason. Sonochem. **62** (2020) 104864, doi: https://doi.org/10.1016/j.ultsonch.2019.104864.

SAŽETAK

Adsorpcija bojila rodamin 6G na mezoporozne materijale Al-MCM-41 i MCM-41

Houda Douba, *Ourida Mohammedi* i *Benamar Cheknane*[*]

Cilj ovog istraživanja bio je procijeniti potencijal mezoporoznih silikata MCM-41 i Al-MCM-41 (molarni omjer Si/Al = 20) za uklanjanje rodamina 6G (Rh6G) iz vodene otopine. Za karakterizaciju adsorbensa primijenjeni su XRD, FTIR, SEM-EDX, BET i UV-Raman. Rezultati XRD analize pokazali su da je struktura MCM-41 nakon ugradnje iona Al ostala netaknuta. Kinetička analiza adsorpcije pokazala je da je u 60. minuti veće uklanjanje Rh6G bojila postignuto uporabom Al-MCM-41 (88,75 %, 26,62 mg g⁻¹). FTIR analiza pokazala je da vodikova veza ima dominantnu ulogu u mehanizmu uklanjanja Rh6G, dok su rezultati pH pokazali da je elektrostatička interakcija također ključni čimbenik. Ovo istraživanje pokazalo je da su pripremljeni mezoporozni materijali jeftini, ali učinkoviti adsorbensi za uklanjanje kationskih boja.

Ključne riječi
Adsorpcija, kationska bojila, izoterme, mezoporozni silikati, rodamin 6G

Laboratory Physical Chemistry of Materials Interfaces Applied to the Environment, University of Saad Dahlab Blida1, 09 000 Blida, Alžir